Available online at www.sciencedirect.com
ScienceDirect
Journal of Sound and Vibration 299 (2007) 460–483
JOURNAL OF SOUND AND VIBRATION
www.elsevier.com/locate/jsvi

Hybrid power flow analysis using coupling loss factor of SEA for low-damping system—Part II: Formulation of 3-D case and hybrid PFFEM

Young-Ho Park, Suk-Yoon Hong*

Department of Naval Architecture and Ocean Engineering, Seoul National University, San 56-1 Sillim-dong, Gwanak-gu, Seoul 151-742, Republic of Korea

Received 5 August 2004; received in revised form 25 January 2006; accepted 27 March 2006
Available online 10 October 2006

Abstract

The hybrid power flow analysis (PFA) is an analytic method proposed for the effective prediction of vibrational and acoustic responses of low-damping system in the medium-to-high frequency ranges by using the PFA algorithm and statistical energy analysis (SEA) coupling concepts. This paper presents the hybrid boundary condition on 3-D case for hybrid PFA in addition to 1-D and 2-D cases which are derived in the other companion paper, and formulates the hybrid power flow finite-element method (PFFEM) including coupling loss factor (CLF) of SEA to extend the application area of hybrid PFA to built-up structures. To verify the derived boundary condition and hybrid PFFEM, numerical analyses were successfully performed for various analytic models and reverberance factors.

1. Introduction

Power flow analysis (PFA) has been developed as a promising tool for predicting vibrational and acoustic responses of built-up structures in the medium-to-high frequency ranges. However, though PFA has the advantage over the traditional finite-element analysis (FEA), boundary element analysis (BEA) and the statistical energy analysis (SEA) in these frequency ranges, the coupling information is somewhat insufficient due to the recent beginning of research and the application of experimental approach is not very easy due to theoretical difficulties [1].

On the other hand, since SEA has been developed by many researchers since 1959 and assumptions in the development of SEA are simplified, SEA has much information especially about the coupling data which are important in the vibro-acoustic analysis of built-up structures and has some commercialized softwares/hardwares calculating SEA parameters such as coupling loss factor (CLF), modal density, damping loss factor, etc. [2]. Therefore, this coupling information can be efficiently used in an alternative method based on energy.

*Corresponding author. Tel.: +82 2 880 8757; fax: +82 2 888 9298.
E-mail address: syh@snu.ac.kr (S.-Y. Hong).

0022-460X/$ - see front matter © 2006 Elsevier Ltd. All rights reserved.
doi:10.1016/j.jsv.2006.03.056

In this paper, the general algorithm for the use of CLF in PFA boundary condition on 3-D case was presented in addition to 1-D and 2-D cases which are derived in the other companion paper [1]. Additionally, the hybrid power flow finite-element method (PFFEM) using the new joint element matrix including CLF was formulated to extend the application area of the developed hybrid PFA to built-up structures and was applied in numerical analyses of built-up structures to evaluate its validity. Finally, using the developed hybrid PFFEM, numerical applications for a simple automobile-shaped structure were represented.

2. Formulation of hybrid boundary condition in PFA

2.1. Three-dimensional case

To extend the scope of the application of hybrid boundary condition which is described in the other companion paper [1], acoustic wave in cavities will be considered as 3-D problem. Bouthier found a second-order energy differential equation for the propagation of acoustic waves in lossy medium [3,4],

$$-\frac{c_{g,a}^2}{\eta\omega}\left(\frac{\partial^2}{\partial x^2}+\frac{\partial^2}{\partial y^2}+\frac{\partial^2}{\partial z^2}\right)\langle e\rangle_a+\eta\omega\langle e\rangle_a=\Pi_{\mathrm{in},a}(x,y,z), \tag{2.1}$$

where $c_{g,a}$ is the group velocity of an acoustic wave in gases, η is the acoustic damping loss factor, ω is the excitation frequency, $\langle e\rangle_a$ is the time- and locally space-averaged acoustic energy density and $\Pi_{\mathrm{in},a}$ is the acoustic power injected by a sound source. The group velocity for acoustic waves is same as the phase speed and is given by

$$c_{g,a}=c_a=\sqrt{\frac{\gamma P_0}{\rho_0}}, \tag{2.2}$$

where γ is the ratio of the specific heats of the gas at constant pressure to the specific heat of the gas at constant volume, P_0 is the standard pressure, and ρ_0 is the density of various gases.

The time- and locally space-averaged acoustic intensity is related to the time- and locally space-averaged acoustic energy density by [4]

$$\langle\vec{I}\rangle_a=-\frac{c_{g,a}^2}{\eta\omega}\left(\frac{\partial}{\partial x}\vec{i}+\frac{\partial}{\partial y}\vec{j}+\frac{\partial}{\partial z}\vec{k}\right)\langle e\rangle_a. \tag{2.3}$$

Like 1- and 2-D cases which are described in the other companion paper, the reverberance factor $\Re_a$ of acoustic wave-field in a subsystem can be defined by

$$\Re_a=\psi_a L_{c,a}, \tag{2.4}$$

where $\psi_a=\eta\omega/c_{g,a}$ and $L_{c,a}$ is the characteristic length of acoustic cavity subsystem.

If the damping loss of acoustic medium like that of the air ($O(10^{-4})$) is very small ($n\ll 1$), the excitation frequency is not very high and the dimension of acoustic cavity is not large, the reverberance factor $\Re_a$ of acoustic wave-field in the subsystem will be very small. In this case, except for the cavity loaded acoustically, the assumption that the energy density field in a acoustic cavity is reverberant ($\langle e\rangle_a=$ constant) is reasonable.

Fig. 1 shows the power flow model of coupled two acoustic cavities of different acoustic properties with no partition. If the acoustic wave-field of each cavity shown in Fig. 1 is reverberant, the power per unit area, which is transferred from the energy of acoustic waves in cavity 1 to cavity 2 using the CLF of SEA, can be expressed as

$$\Pi_{1a\to 2a}=\frac{\omega\eta_{12}E_{1a}}{S}=\frac{\omega\eta_{12}V_1\langle e_1\rangle_a}{S}, \tag{2.5}$$

where E_{1a} is the total energy, V_1 is the volume of acoustic cavity 1, η_{12} is the CLF from cavity 1 to cavity 2, S is the area of area junction, and $\langle e\rangle_a$ is the energy density of acoustic wave in cavity 1. The CLF for area junction between two acoustic cavities is known as [2]

$$\eta_{12}=\frac{c_{g1,a}S\langle\tau\rangle_{12}}{4\omega V_1}, \tag{2.6}$$

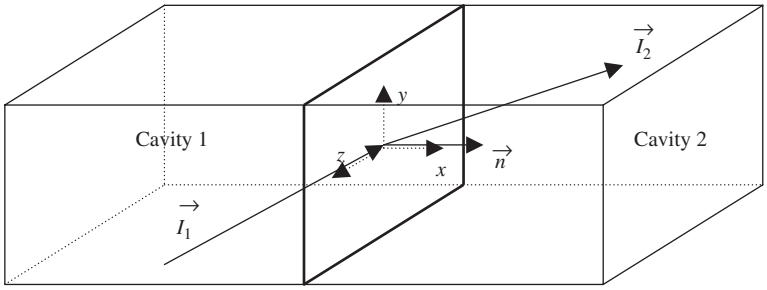

Fig. 1. Power flow model of coupled two cavities.

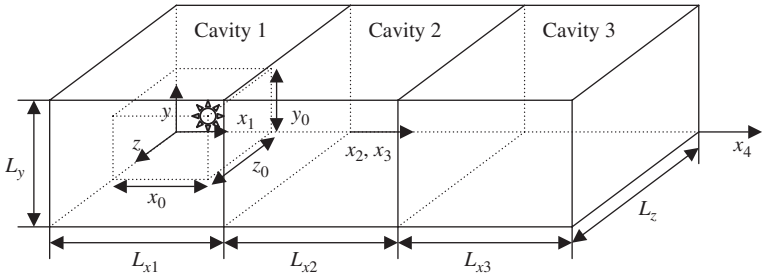

Fig. 2. Coupled acoustic cavities without partitions.

where $c_{g1,a}$ is the group velocity of acoustic waves in cavity 1, $\langle \tau \rangle_{12}$ is the diffuse power transmission coefficient from cavity 1 to cavity 2. Using Eqs. (2.3) and (2.5), the net power of the acoustic wave from cavity 1 to cavity 2 can be represented as

$$\Pi_{12} = -\frac{c_{g1a}^2}{\eta_1 \omega} \nabla \langle e \rangle_{1a} \cdot \vec{n} = -\frac{c_{g2a}^2}{\eta_2 \omega} \nabla \langle e \rangle_{2a} \cdot \vec{n} = (\Pi_{1\to 2} - \Pi_{2\to 1}) = \frac{\omega}{S} \left(V_1 \eta_{12} \langle e_1 \rangle_a - V_2 \eta_{21} \langle e_2 \rangle_a \right), \tag{2.7}$$

where $\vec{n}$ is the normal vector shown in Fig. 1.

In the model shown in Fig. 1, regardless of the reverberance factor, the classical boundary conditions of power flow solutions for acoustic wave can be expressed as

$$\langle q_2 \rangle_{a,x}^{+} = \tau_{12} \langle q_1 \rangle_{a,x}^{+} + \gamma_{22} \langle q_2 \rangle_{a,x}^{-} \tag{2.8}$$

and

$$\langle q_1 \rangle_{a,x}^{-} = \gamma_{11} \langle q_1 \rangle_{a,x}^{+} + \tau_{21} \langle q_2 \rangle_{a,x}^{-}, \tag{2.9}$$

where $\langle q_i \rangle_{a,x}^{+}$ is the x-component of acoustic intensity in the $+x$-direction, τ and γ are the diffuse power transmission and reflection coefficients of acoustic waves, respectively. The evaluation of diffuse power transmission and reflection coefficients for coupled acoustic spaces is discussed in Appendix B.

2.1.1. Numerical examples

The numerical applications of hybrid method on 3-D case are performed for ideally coupled three acoustic cavities shown in Fig. 2. Each cavity has the same dimension of $L_{x1} = L_{x2} = L_{x3} = L_y = L_z = 1\,\text{m}$. The acoustic properties of each cavity are assumed to be $\rho_1 = 1.3\,\text{kg/m}^3$, $c_1 = 330\,\text{m/s}$, $\rho_2 = 1.35\,\text{kg/m}^3$, $c_2 = 340\,\text{m/s}$, $\rho_3 = 1.37\,\text{kg/m}^3$ and $c_3 = 350\,\text{m/s}$. Acoustic input power is located at $x_0 = L_{x1}/2$, $y_0 = L_y/2$ and $z_0 = L_z/2$ in cavity 1 and its magnitude is $P = 10\,\text{W}$. The detail procedure of the numerical analysis on 3-D case is discussed in Appendix A. Figs. 3–6 show 3-D power flow solutions along the plane $z = 0.5\,L_z$ when the excitation frequency is $f = 5\,\text{kHz}$. In the numerical model of Figs. 3 and 4, the acoustic damping loss factors of all cavities were assumed to be 0.001 and the reverberance

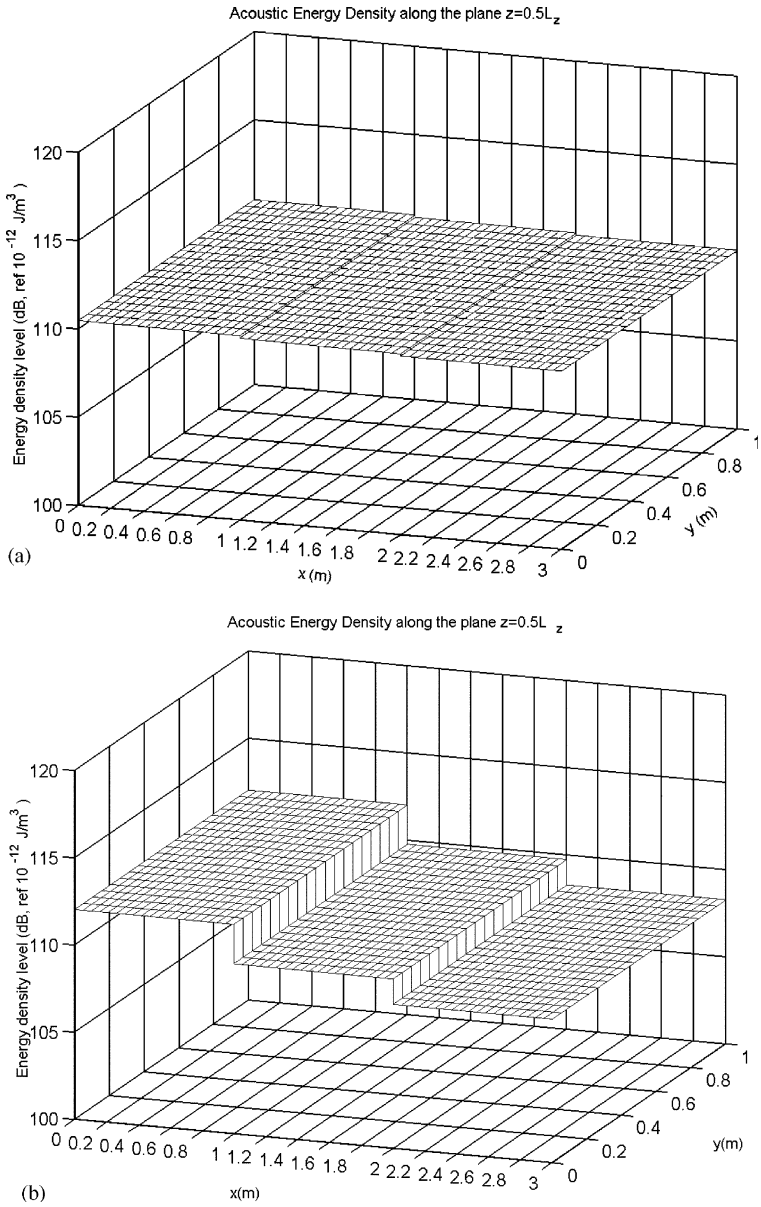

Fig. 3. Acoustic energy density level along the plane $z = 0.5\,L_z$ in $f = 5$ kHz, $\eta_1 = \eta_2 = \eta_3 = 0.001$: (a) using classical boundary condition at all area junctions; and (b) using hybrid boundary condition at all area junctions.

factors of acoustic wave-fields in each cavity are $\Re_{a1} = 0.1649$, $\Re_{a2} = 0.16$ and $\Re_{a3} = 0.1555$, respectively. In Figs. 5 and 6, the acoustic damping loss factors of all cavities were assumed to be 0.0001 and the reverberance factors of acoustic wave-fields in each cavity are $\Re_{a1} = 0.0165$, $\Re_{a2} = 0.016$ and $\Re_{a3} = 0.0156$, respectively. In Figs. 3–6, the sub-figures (a) and (b) of each figure are the power flow solutions using the classical boundary condition represented in Eqs. (2.8) and (2.9), and the hybrid boundary condition represented in Eq. (2.7) in all area junctions, respectively. The diffuse acoustic power transmission and reflection coefficients used in two area junctions are evaluated numerically (Appendix B). In the sub-figure (b) of Figs. 3–6, though the hybrid boundary condition using CLF of SEA is applied at all area junctions, the spatial variations of acoustic energy densities and intensities appear well. Additionally, because the reverberance factors of acoustic wave-fields in the numerical model of Fig. 3 are broken down into those as large as in Fig. 5, the energy density level using

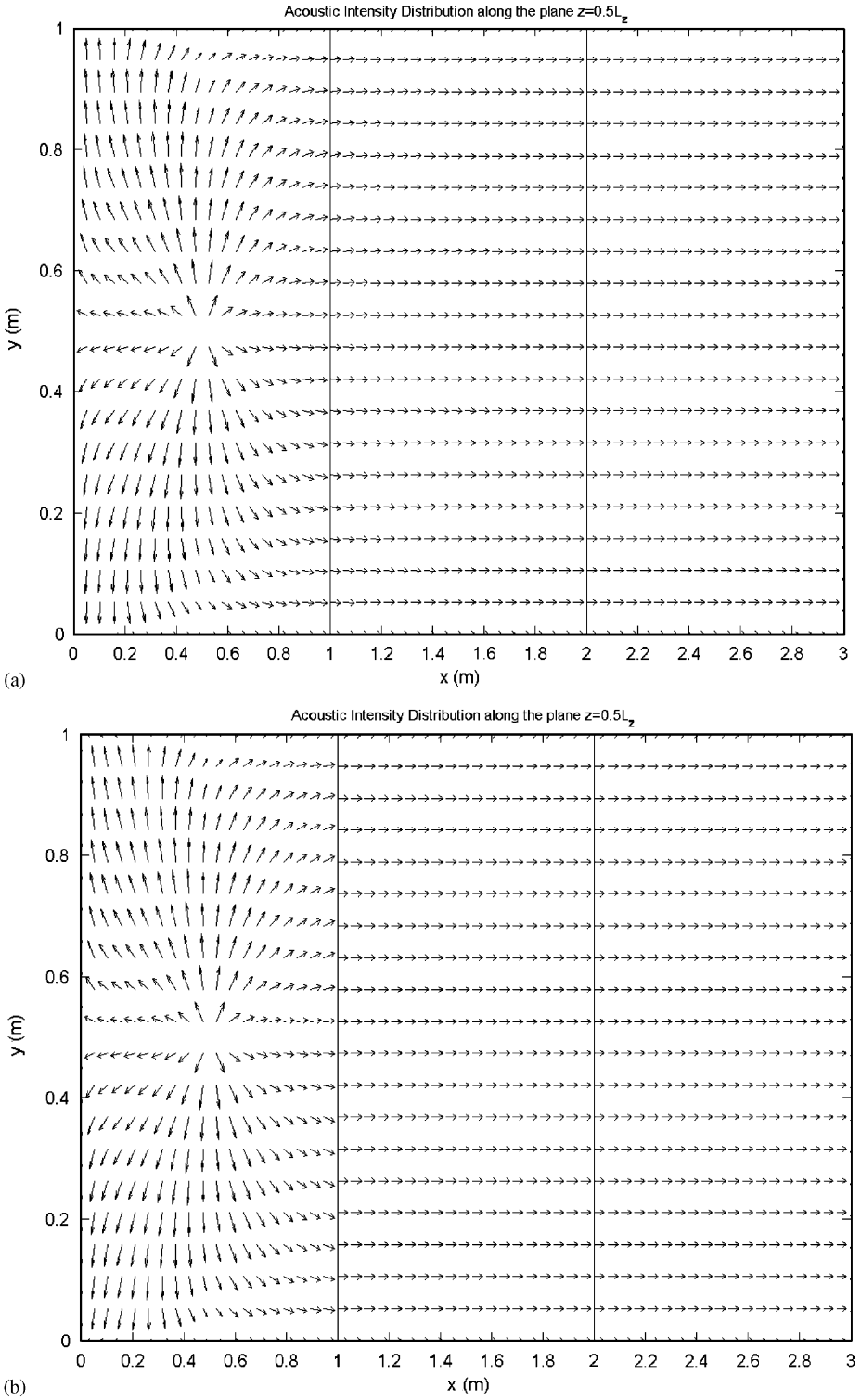

Fig. 4. Acoustic intensity distribution along the plane $z = 0.5\,L_z$ in $f = 5\,\text{kHz}$, $\eta_1 = \eta_2 = \eta_3 = 0.001$: (a) using classical boundary condition at all area junctions; and (b) using hybrid boundary condition at all area junctions.

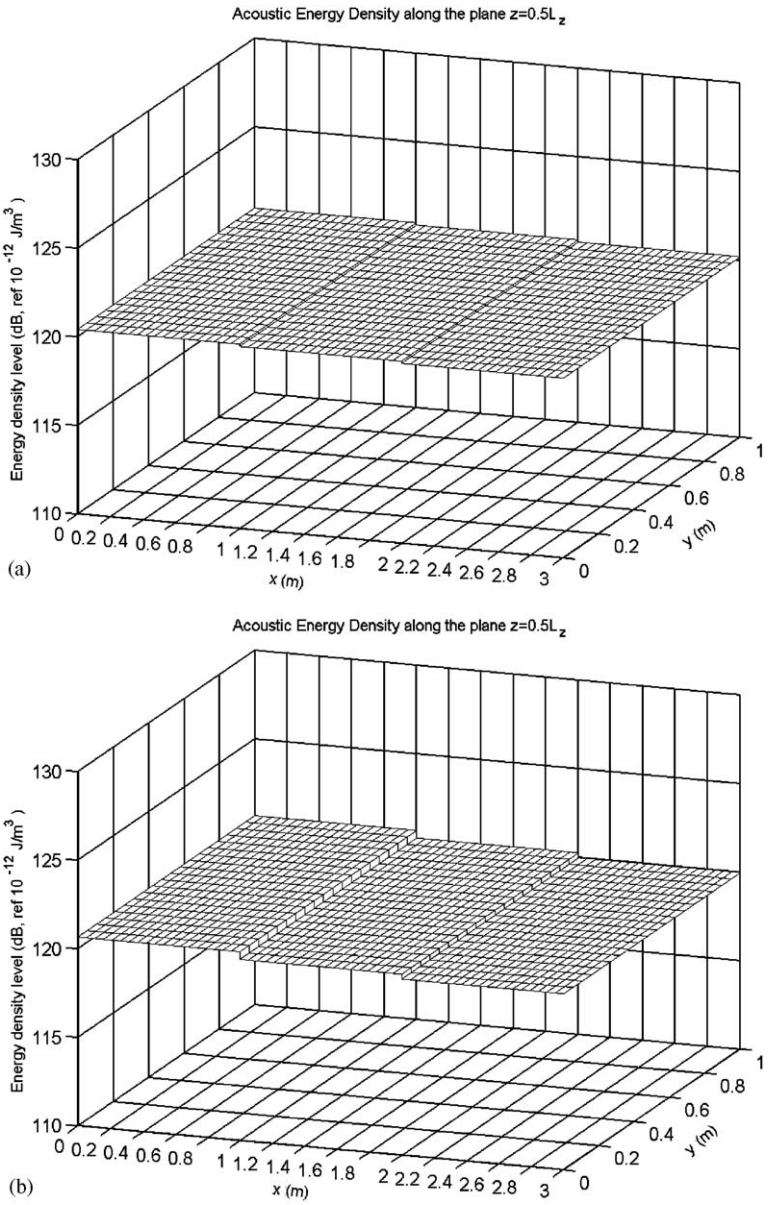

Fig. 5. Acoustic energy density level along the plane $z = 0.5\,L_z$ in $f = 5$ kHz, $\eta_1 = \eta_2 = \eta_3 = 0.0001$: (a) using classical boundary condition at all area junctions; and (b) using hybrid boundary condition at all area junctions.

classical boundary condition is somewhat different from that using hybrid boundary condition in Fig. 3 and the difference between those is within 2 dB. However, the energy density levels using classical and hybrid boundary conditions show a good agreement in Fig. 5 due to relatively small reverberance factors. For the in-depth confirmation of the effect of reverberance factor, Fig. 7 shows the relative difference between space-averaged acoustic energy densities obtained using hybrid boundary condition and classical boundary condition, divided by the space-averaged energy density using classical boundary condition $\left(\|\overline{E_{3,\,\mathrm{classic}}} - \overline{E_{3,\,\mathrm{hybrid}}}\|/\|\overline{E_{3,\,\mathrm{classic}}}\|\right)$ in cavity 3. Like previous 1- and 2-D cases, as the reverberance factor of acoustic wave-field in cavity 3 decreases, the power flow solutions using each boundary condition on 3-D case become nearly equal.

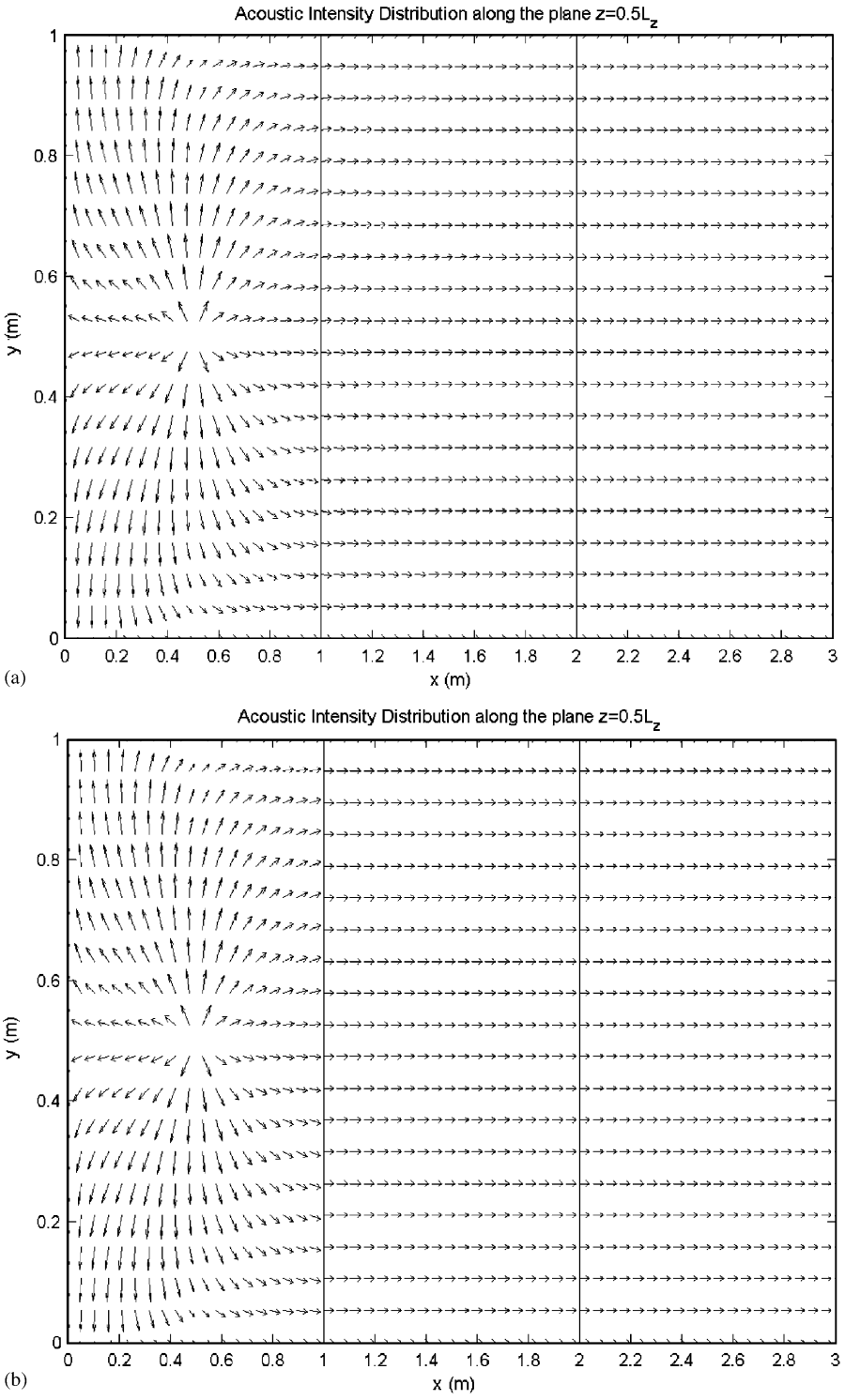

Fig. 6. Acoustic intensity distribution along the plane $z = 0.5\,L_z$ in $f = 5\,\text{kHz}$, $\eta_1 = \eta_2 = \eta_3 = 0.0001$: (a) using classical boundary condition at all area junctions; and (b) using hybrid boundary condition at all area junctions.

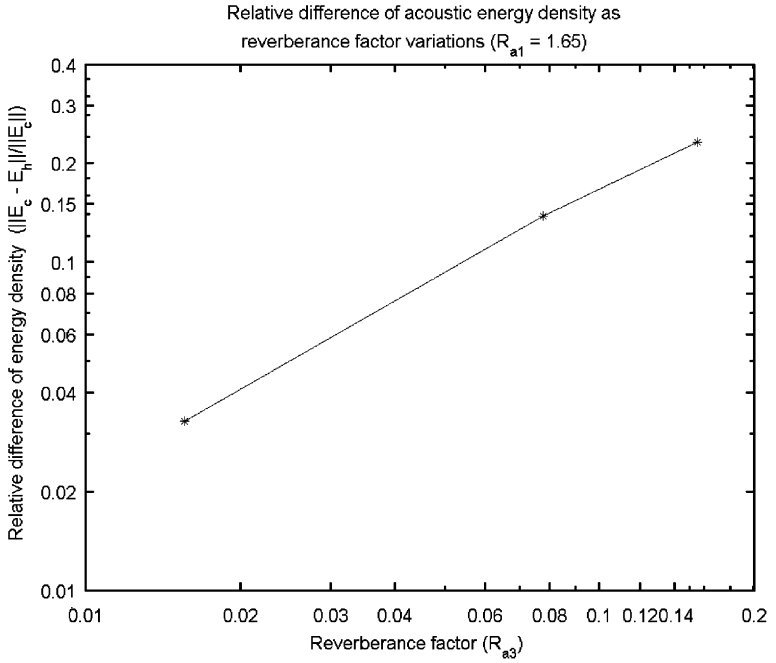

Fig. 7. Relative difference $\left(||\overline{E_c} - \overline{E_h}||/||\overline{E_c}||\right)$ between space-averaged acoustic energy densities of cavity 3, using classical and hybrid boundary conditions as the reverberance factor variation of cavity 3 in $f = 5\,\text{kHz}$ and $\Re_{a1} = 1.65$.

3. Formulation of hybrid PEFEM

For PFA of built-up structures, the numerical approach such as the finite element and boundary element techniques is required for obtaining the power flow solution of energy governing equation. Nefske and Sung implemented a finite element formulation of the energy governing equation and the developed PFFEM was used to predict the vibrational response of beam structures [5]. Cho presented the finite element formulations for 1-D energy equation considering multi-degrees-of-freedom and 2-D energy equation considering one degree-of-freedom [6]. Seo expanded into the general finite element formulation for the 2-D case [7]. Recently, Seo and Park developed the software for vibration analysis, PFA design system (PFADS), based on PFFEM [8,9].

In this paper, the hybrid power flow finite element (PFFE) formulation using CLF of SEA was represented and the hybrid PFFEM on a typical 2-D case was considered. For the hybrid PFFEM using CLF of SEA, the derivation of new joint element matrix used for linearization of the global matrix equation is required.

For the hybrid PFFE formulation of 2-D energy governing equation, the weak variational form of energy governing equation for the propagation of "m"-type wave is obtained and the following equation is obtained by Galerkin weighted residual approximation:

$$\sum_{j=1}^{n}\left\{\int_D\left(\frac{c_{gm}^2}{\eta\omega}\nabla\phi_i\cdot\nabla\phi_j+\eta\omega\phi_i\phi_j\right)\mathrm{d}D\right\}e_j=\int_D \Pi_m\phi_i\,\mathrm{d}D+\int_\Gamma \phi_i\{(-v)\cdot\langle\vec{I}\rangle_m\}\,\mathrm{d}\Gamma, \tag{3.1}$$

where c_{gm} is the group velocity of "m"-type wave, e_j is the nodal value of energy density, ϕ_i is the basis function for energy density approximation $\left(\langle e\rangle_m=\sum_{j=1}^{n}e_j\phi_j\right)$, v is a unit vector normal to the domain boundary Γ, n is the number of the basis functions and the intensity of "m"-type wave in the boundary is $\langle\vec{I}\rangle_m=-c_{gm}^2\nabla e_m/\eta\omega$.

Eq. (3.1) can be written in element matrix form as [6]

$$\left[K^{(e)}\right]\left\{e^{(e)}\right\}=\left\{F^{(e)}\right\}+\left\{Q^{(e)}\right\}, \tag{3.2}$$

where

$$K_{m,ij}^{(e)} = \int_D \left(\frac{c_{gm}^2}{\eta\omega} \nabla\phi_i \cdot \nabla\phi_j + \eta\omega\phi_i\phi_j \right) \mathrm{d}D,$$

$$F_{m,i}^{(e)} = \int_D \Pi_m \phi_i \, \mathrm{d}D,$$

$$Q_{m,i}^{(e)} = \int_\Gamma \phi_i \left\{ (-v) \cdot \langle \vec{I} \rangle_m \right\} \mathrm{d}\Gamma$$

and

$$\left\{ e^{(e)} \right\} = \left\{ e_1^{(e)} \; e_2^{(e)} \; \ldots \; e_n^{(e)} \right\}^{\mathrm{T}} \quad (i,j = 1,2,\ldots,n).$$

In Eq. (3.2), the negative sign of $Q_{m,i}^{(e)}$ term means the net power flux of the inner-direction of element.

When the element matrix equations of all elements are acquired, global matrix equation has to be assembled to solve the linear equation. The global matrix equation can be represented as

$$[K]\{e\} = \{F\} + \{Q\}. \tag{3.3}$$

First of all, if the terms on only "m"-type wave are considered, the matrix $\{Q\}$, the global power flow matrix, includes the differential terms of the energy density and can be expanded to

$$\{Q_m\} = \left\{ \ldots, \; Q_m^{(k)}, \; Q_m^{(k+1)}, \ldots \right\}^{\mathrm{T}}, \tag{3.4}$$

where

$$Q_m^{(k)} = \left\{ Q_{m1}^{(k)}, \ldots, Q_{mn}^{(k)} \right\} = \left\{ \int_{\Gamma_k} \phi_1^{(k)} q_m^{(k)} \, \mathrm{d}\Gamma_k, \ldots, \; \int_{\Gamma_k} \phi_n^{(k)} q_m^{(k)} \, \mathrm{d}\Gamma_k \right\} \tag{3.5}$$

and

$$Q_m^{(k+1)} = \left\{ Q_{m1}^{(k+1)}, \ldots, Q_{mn}^{(k+1)} \right\} = \left\{ \int_{\Gamma_{k+1}} \phi_1^{(k+1)} q_m^{(k+1)} \, \mathrm{d}\Gamma_{k+1}, \ldots, \; \int_{\Gamma_{k+1}} \phi_n^{(k+1)} q_m^{(k+1)} \, \mathrm{d}\Gamma_{k+1} \right\}, \tag{3.6}$$

where $Q_m^{(k)}$ and $Q_m^{(k+1)}$ are the "m"-type boundary energy flux vectors for two adjacent boundary elements, k and $k+1$, respectively, lying on the line joint of two elements [6]. The general hybrid boundary condition on 2-D case, which is described in the other companion paper, can be represented as [1]

$$-\frac{c_{gif}^2}{\eta_i\omega} \nabla\langle e_i \rangle_f \cdot \vec{n}_i = \sum_{j=1,\, j\neq i}^{N} \left[\sum_{m=f,\, l,\, s} \left\{ \frac{\omega}{L} \left(S_i \eta_{ijfm} \langle e_i \rangle_f - S_j \eta_{jimf} \langle e_j \rangle_m \right) \right\} \right] \quad (i = 1,\ldots,N), \tag{3.7}$$

$$-\frac{c_{gil}^2}{\eta_i\omega} \nabla\langle e_i \rangle_l \cdot \vec{n}_i = \sum_{j=1,\, j\neq i}^{N} \left[\sum_{m=f,\, l,\, s} \left\{ \frac{\omega}{L} \left(S_i \eta_{ijlm} \langle e_i \rangle_l - S_j \eta_{jiml} \langle e_j \rangle_m \right) \right\} \right] \quad (i = 1,\ldots,N), \tag{3.8}$$

and

$$-\frac{c_{gis}^2}{\eta_i\omega} \nabla\langle e_i \rangle_s \cdot \vec{n}_i = \sum_{j=1,\, j\neq i}^{N} \left[\sum_{m=f,\, l,\, s} \left\{ \frac{\omega}{L} \left(S_i \eta_{ijsm} \langle e_i \rangle_s - S_j \eta_{jims} \langle e_j \rangle_m \right) \right\} \right] \quad (i = 1,\ldots,N), \tag{3.9}$$

where $-(c_{gim}^2/\eta_i\omega)\nabla\langle e_i \rangle_m \cdot \vec{n}_i$ is net "m"-type power in plate i, $\langle e_i \rangle_m$ is "m"-type energy density of plate i, η_{ijmn} is CLF form "m"-type waves in plate i to "n"-type waves in plate j, S_i is the area of plate i, L is the length of line junction among plates and $\vec{n}_i$ is the normal vector of line junction in plate i.

Substituting the hybrid boundary condition given in Eqs. (3.7)–(3.9) into Eq. (3.4), the joint power flow equations can be expressed as, using CLF of SEA,

$$q_m^{(k)} = p_{(k+1)(k)} - p_{(k)(k+1)} = \frac{\omega}{L^2}\left\{-S_{(k)}\eta_{(k)(k+1)mm}e_m^{(k)} + S_{(k+1)}\eta_{(k+1)(k)mm}e_m^{(k+1)}\right\} \tag{3.10}$$

and

$$q_m^{(k+1)} = p_{(k)(k+1)} - p_{(k+1)(k)} = \frac{\omega}{L^2}\left\{S_{(k)}\eta_{(k)(k+1)mm}e_m^{(k)} - S_{(k+1)}\eta_{(k+1)(k)mm}e_m^{(k+1)}\right\}, \tag{3.11}$$

where $S_{(k)}$ is the area of the element including boundary element k, L is the total length of line junction and $\eta_{(k)(k+1)mm}$ is the CLF between the "m"-type energies of elements including boundary elements k and $k+1$. The values of the energy density in the boundary element can be approximated as, using the basis functions corresponding to boundary nodes,

$$e_m^{(k)} = \sum_{j=1}^{n} \phi_j e_{mj}^{(k)}, \tag{3.12}$$

where $e_{mj}^{(k)}$ are nodal values of "m"-type energy density of the boundary element k, ϕ_j are the basis functions, and the integer, n, is the number of the basis function. Using Eqs. (3.10) and (3.11), the global power flow matrix in Eq. (3.4) can be written by

$$\begin{Bmatrix} \vdots \\ Q_m^{(k)} \\ Q_m^{(k+1)} \\ \vdots \end{Bmatrix} = \frac{\omega}{L^2}\begin{Bmatrix} \vdots \\ -S_{(k)}\eta_{(k)(k+1)mm}\sum_{j=1}^{n}\left(e_{mj}^{(k)}\oint_\Gamma \phi_i\phi_j\,\mathrm{d}\Gamma\right) + S_{(k+1)}\eta_{(k+1)(k)mm}\sum_{j=1}^{n}\left(e_{mj}^{(k+1)}\oint_\Gamma \phi_i\phi_j\,\mathrm{d}\Gamma\right) \\ S_{(k)}\eta_{(k)(k+1)mm}\sum_{j=1}^{n}\left(e_{mj}^{(k)}\oint_\Gamma \phi_i\phi_j\,\mathrm{d}\Gamma\right) - S_{(k+1)}\eta_{(k+1)(k)mm}\sum_{j=1}^{n}\left(e_{mj}^{(k+1)}\oint_\Gamma \phi_i\phi_j\,\mathrm{d}\Gamma\right) \\ \vdots \end{Bmatrix}. \tag{3.13}$$

To illustrate the global matrix assembly procedure, the example shown in Fig. 8 is considered. In Fig. 8, the global nodes are not real finite element nodes. In a common finite element model, the model composed of two coupled quadrilateral elements is modeled with six-nodes. However, as known, because the discontinuity of energy density in PFA occurs in the coupled line junction, two virtual nodes have to be added and the numbers of total nodes renumbered as shown in Fig. 8. In case of the example shown in Fig. 8, Eq. (3.13) can be

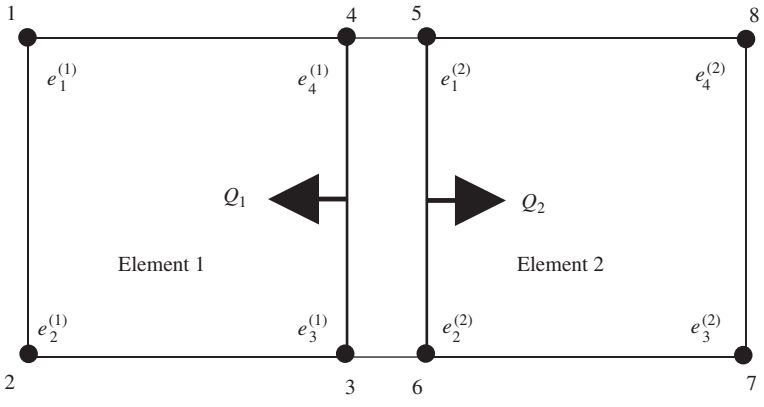

Fig. 8. Two four-node quadrilateral elements for power flow finite element method.

expressed as, with the nodal values of boundary nodes, i.e., 3–6,

$$\begin{Bmatrix} Q_{m3} \\ Q_{m4} \\ Q_{m6} \\ Q_{m5} \end{Bmatrix} = \frac{\omega l}{L^2} \begin{Bmatrix} -S_1\eta_{12\,\mathrm{mm}} \begin{bmatrix} 1/3 & 1/6 \\ 1/6 & 1/3 \end{bmatrix} \begin{Bmatrix} e_{m3}^{(1)} \\ e_{m4}^{(1)} \end{Bmatrix} + S_2\eta_{21\,\mathrm{mm}} \begin{bmatrix} 1/3 & 1/6 \\ 1/6 & 1/3 \end{bmatrix} \begin{Bmatrix} e_{m2}^{(2)} \\ e_{m1}^{(2)} \end{Bmatrix} \\ S_1\eta_{12\,\mathrm{mm}} \begin{bmatrix} 1/3 & 1/6 \\ 1/6 & 1/3 \end{bmatrix} \begin{Bmatrix} e_{m3}^{(1)} \\ e_{m4}^{(1)} \end{Bmatrix} - S_2\eta_{21\,\mathrm{mm}} \begin{bmatrix} 1/3 & 1/6 \\ 1/6 & 1/3 \end{bmatrix} \begin{Bmatrix} e_{m2}^{(2)} \\ e_{m1}^{(2)} \end{Bmatrix} \end{Bmatrix} = [J] \begin{Bmatrix} e_{m3} \\ e_{m4} \\ e_{m6} \\ e_{m5} \end{Bmatrix}, \quad (3.14)$$

where l is the length of line junction in one element.

Considering full degrees-of-freedom (flexural, longitudinal and shear waves) in a plate, Eq. (3.13) can be expanded into

$$\begin{Bmatrix} \vdots \\ Q_f^{(k)} \\ Q_f^{(k+1)} \\ Q_l^{(k)} \\ Q_l^{(k+1)} \\ Q_s^{(k)} \\ Q_s^{(k+1)} \\ \vdots \end{Bmatrix} = \frac{\omega}{L^2} \begin{Bmatrix} \vdots \\ -S_{(k)} \left\{ \sum_{p=f,\,l,\,s} \left(\eta_{(k)\,(k+1)fp} \right) \right\} \left\{ \sum_{j=1}^{n} \left(e_{f,j}^{(k)} \oint_\Gamma \phi_i \phi_j \, \mathrm{d}\Gamma \right) \right\} + S_{(k+1)} \left\{ \sum_{p=f,\,l,\,s} \left(\eta_{(k+1)\,(k)pf} \left\{ \sum_{j=1}^{n} \left(e_{p,j}^{(k+1)} \oint_\Gamma \phi_i \phi_j \, \mathrm{d}\Gamma \right) \right\} \right) \right\} \\ S_{(k)} \left\{ \sum_{p=f,\,l,\,s} \left(\eta_{(k)\,(k+1)pf} \left\{ \sum_{j=1}^{n} \left(e_{p,j}^{(k)} \oint_\Gamma \phi_i \phi_j \, \mathrm{d}\Gamma \right) \right\} \right) \right\} - S_{(k+1)} \left\{ \sum_{p=f,\,l,\,s} \left(\eta_{(k+1)\,(k)fp} \right) \right\} \left\{ \sum_{j=1}^{n} \left(e_{f,j}^{(k+1)} \oint_\Gamma \phi_i \phi_j \, \mathrm{d}\Gamma \right) \right\} \\ -S_{(k)} \left\{ \sum_{p=f,\,l,\,s} \left(\eta_{(k)\,(k+1)lp} \right) \right\} \left\{ \sum_{j=1}^{n} \left(e_{l,j}^{(k)} \oint_\Gamma \phi_i \phi_j \, \mathrm{d}\Gamma \right) \right\} + S_{(k+1)} \left\{ \sum_{p=f,\,l,\,s} \left(\eta_{(k+1)\,(k)pl} \left\{ \sum_{j=1}^{n} \left(e_{p,j}^{(k+1)} \oint_\Gamma \phi_i \phi_j \, \mathrm{d}\Gamma \right) \right\} \right) \right\} \\ S_{(k)} \left\{ \sum_{p=f,\,l,\,s} \left(\eta_{(k)\,(k+1)pl} \left\{ \sum_{j=1}^{n} \left(e_{p,j}^{(k)} \oint_\Gamma \phi_i \phi_j \, \mathrm{d}\Gamma \right) \right\} \right) \right\} - S_{(k+1)} \left\{ \sum_{p=f,\,l,\,s} \left(\eta_{(k+1)\,(k)lp} \right) \right\} \left\{ \sum_{j=1}^{n} \left(e_{l,j}^{(k+1)} \oint_\Gamma \phi_i \phi_j \, \mathrm{d}\Gamma \right) \right\} \\ -S_{(k)} \left\{ \sum_{p=f,\,l,\,s} \left(\eta_{(k)\,(k+1)sp} \right) \right\} \left\{ \sum_{j=1}^{n} \left(e_{s,j}^{(k)} \oint_\Gamma \phi_i \phi_j \, \mathrm{d}\Gamma \right) \right\} + S_{(k+1)} \left\{ \sum_{p=f,\,l,\,s} \left(\eta_{(k+1)\,(k)ps} \left\{ \sum_{j=1}^{n} \left(e_{p,j}^{(k+1)} \oint_\Gamma \phi_i \phi_j \, \mathrm{d}\Gamma \right) \right\} \right) \right\} \\ S_{(k)} \left\{ \sum_{p=f,\,l,\,s} \left(\eta_{(k)\,(k+1)ps} \left\{ \sum_{j=1}^{n} \left(e_{p,j}^{(k)} \oint_\Gamma \phi_i \phi_j \, \mathrm{d}\Gamma \right) \right\} \right) \right\} - S_{(k+1)} \left\{ \sum_{p=f,\,l,\,s} \left(\eta_{(k+1)\,(k)sp} \right) \right\} \left\{ \sum_{j=1}^{n} \left(e_{s,j}^{(k+1)} \oint_\Gamma \phi_i \phi_j \, \mathrm{d}\Gamma \right) \right\} \\ \vdots \end{Bmatrix}, \quad (3.15)$$

where $e_{m,j}^{(k)}$ is the nodal value of "m"-type energy in boundary element k, and $\eta_{(k)(k+1)mp}$ is CLF from "m"-type energy in boundary element k to "p"-type energy in boundary element $k+1$. Using Eq. (3.15), Eq. (3.14) can be expanded as

$$\begin{Bmatrix} Q_{f3} \\ Q_{f4} \\ Q_{f6} \\ Q_{f5} \\ Q_{l3} \\ Q_{l4} \\ Q_{l6} \\ Q_{l5} \\ Q_{s3} \\ Q_{s4} \\ Q_{s6} \\ Q_{s5} \end{Bmatrix} = \frac{\omega}{L^2} \begin{Bmatrix} -S_1 \left(\sum_{p=f,\,l,\,s} \eta_{12fp} \right) [m_1] & S_2\eta_{21ff}[m_2] & 0 & S_2\eta_{21lf}[m_2] & 0 & S_2\eta_{21sf}[m_2] \\ S_1\eta_{12ff}[m_1] & -S_2 \left(\sum_{p=f,\,l,\,s} \eta_{21fp} \right) [m_2] & S_1\eta_{12lf}[m_1] & 0 & S_1\eta_{12sf}[m_1] & 0 \\ 0 & S_2\eta_{21fl}[m_2] & -S_1 \left(\sum_{p=f,\,l,\,s} \eta_{12lp} \right) [m_1] & S_2\eta_{21ll}[m_2] & 0 & S_2\eta_{21sl}[m_2] \\ S_1\eta_{12fl}[m_1] & 0 & S_1\eta_{12ll}[m_1] & -S_2 \left(\sum_{p=f,\,l,\,s} \eta_{21lp} \right) [m_2] & S_1\eta_{12sl}[m_1] & 0 \\ 0 & S_2\eta_{21fs}[m_2] & 0 & S_2\eta_{21ls}[m_2] & -S_1 \left(\sum_{p=f,\,l,\,s} \eta_{12sp} \right) [m_1] & S_2\eta_{21ss}[m_2] \\ S_1\eta_{12fs}[m_1] & 0 & S_1\eta_{12ls}[m_1] & 0 & S_1\eta_{12ss}[m_1] & -S_2 \left(\sum_{p=f,\,l,\,s} \eta_{21sp} \right) [m_2] \end{Bmatrix} \begin{Bmatrix} e_{f3} \\ e_{f4} \\ e_{f6} \\ e_{f5} \\ e_{l3} \\ e_{l4} \\ e_{l6} \\ e_{l5} \\ e_{s3} \\ e_{s4} \\ e_{s6} \\ e_{s5} \end{Bmatrix}, \quad (3.16)$$

where $[m_1]$ and $[m_2]$ can be represented as

$$[m_1] = [m_2] = \frac{l}{6} \begin{bmatrix} 2 & 1 \\ 1 & 2 \end{bmatrix}$$

with the length of boundary in one element, l. The new joint element Eq. (3.16) can be simply expressed as

$$\begin{Bmatrix} Q_f \\ Q_l \\ Q_s \end{Bmatrix} = [J_h] \begin{Bmatrix} e_f \\ e_l \\ e_s \end{Bmatrix}, \tag{3.17}$$

where $[J_h]$ is the new joint element matrix for hybrid PFFEM using CLF of SEA.

The new global matrix equation can be assembled as

$$\left(\begin{bmatrix} K_f & & \\ & K_l & \\ & & K_s \end{bmatrix} - [J_h] \right) \begin{Bmatrix} e_f \\ e_l \\ e_s \end{Bmatrix} = \begin{Bmatrix} \Pi_f \\ \Pi_l \\ \Pi_s \end{Bmatrix}. \tag{3.18}$$

3.1. Numerical examples

To validate the new joint element formulation for hybrid PFFEM, the model composed of coupled two plates is applied. The dimension and thickness of each plate shown in Fig. 9 are $L_x = L_y = 1\,\text{m}$ and $h = 1\,\text{mm}$, respectively, and the material properties of the structure were assumed to be the same as those of steel ($E = 19.5 \times 10^{10}\,\text{Pa}$, $\rho = 7800\,\text{kg/m}^3$). The force is located at the center of one plate and its amplitude is $F = 100\,\text{N}$. The angle between two plates is 90°. The structural loss factor for two plates was assumed to be 0.1. Fig. 9 shows the finite element model of a plate structure for numerical applications. The finite element model shown in Fig. 9 has 200 elements, 231 nodes and 726 degrees-of-freedom. Figs. 10 and 11 show the energy density level and intensity level distributions of each wave obtained by hybrid PFFEM in $f = 1\,\text{kHz}$, respectively.

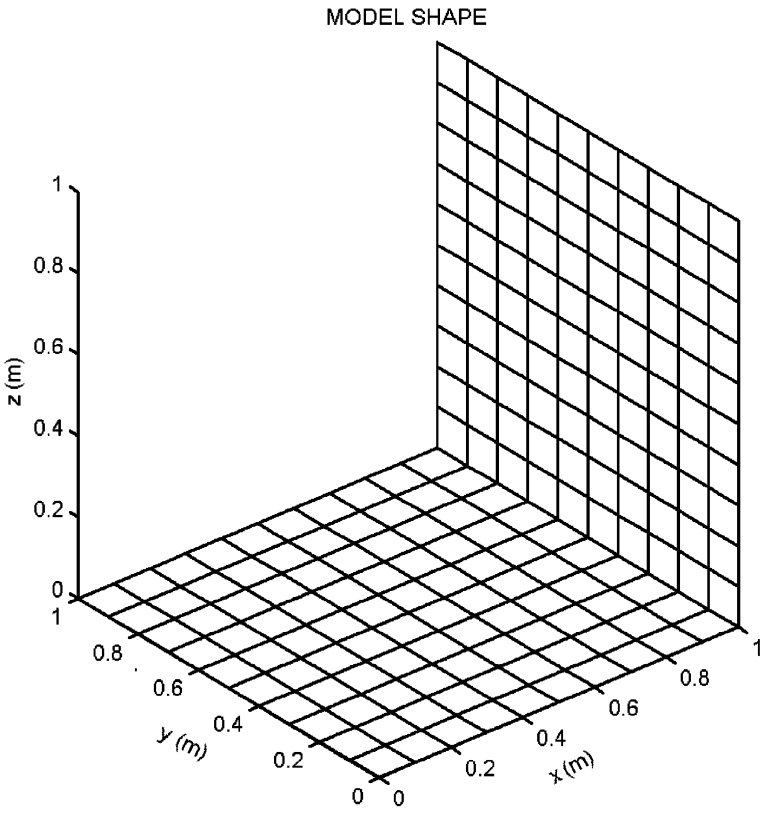

Fig. 9. Finite element model of coupled plates for hybrid PFFEM.

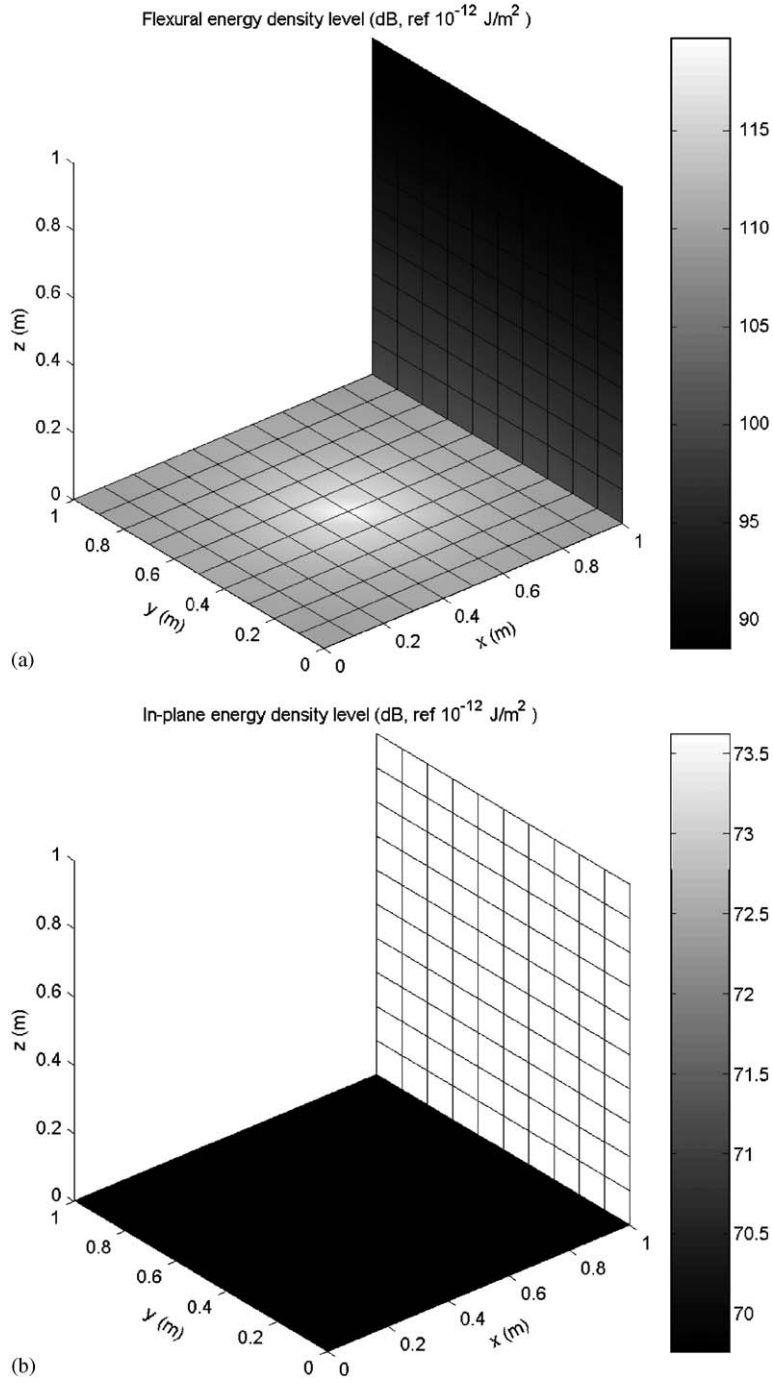

Fig. 10. Energy density level of hybrid PFFEM when $f = 1$ kHz and $\eta = 0.1$: (a) flexural energy; and (b) in-plane energy.

Though the CLF of SEA is used in the joint element matrix, the spatial variations of energy density and intensity within one subsystem appear successfully. Fig. 12 shows the comparison between the analytic power flow solution using hybrid boundary condition and the numerical power flow solution by hybrid PFFEM in $y = 0.5$ m. As expected, the numerical results by two methods agree well as shown in Fig. 12. By these results, the hybrid PFFEM using the new joint element matrix including CLF of SEA was successively validated.

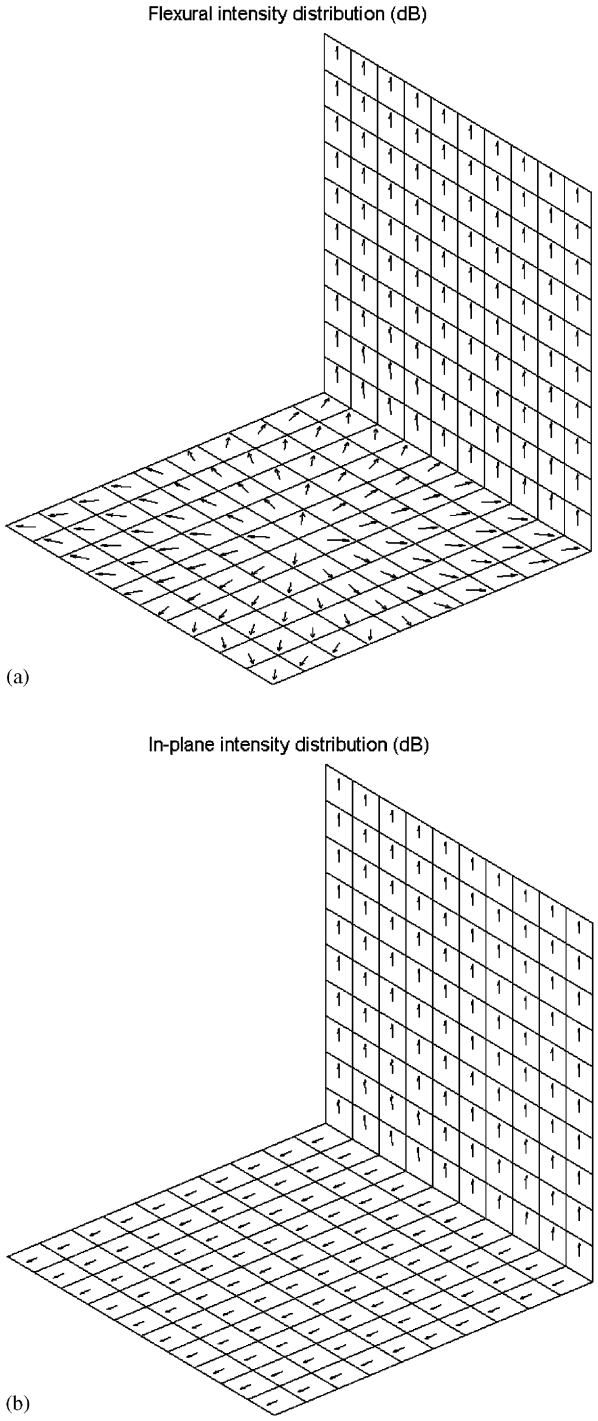

Fig. 11. Intensity distribution of hybrid PFFEM when $f = 1$ kHz and $\eta = 0.1$: (a) flexural energy, and (b) in-plane energy.

To expand the region of application of hybrid PFFEM to built-up structures, an additional example is presented. Fig. 13 shows the finite element model of an automobile-shaped structure, consisting of 706 nodes, 704 elements and 2616 degrees-of-freedom. The material properties were assumed to be those of steel and the thickness of all plates is 0.001 m. Figs. 14 and 15 show the numerical results of hybrid PFFEM and classical

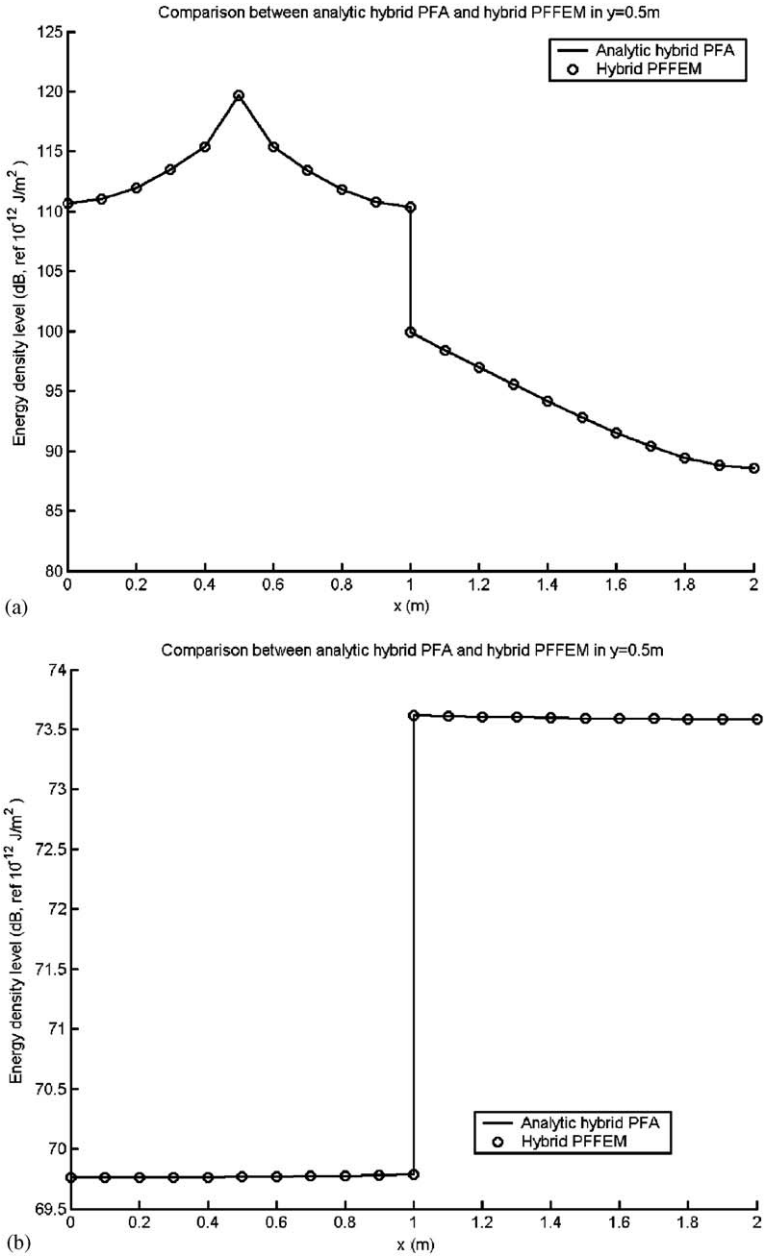

Fig. 12. Comparison between analytic hybrid PFA and hybrid PFFEM when $f = 1$ kHz and $\eta = 0.01$: (a) flexural energy; and (b) in-plane energy.

PFFEM, respectively, when $f = 200$ Hz and $\eta = 0.0001$. Additionally, Figs. 16 and 17 show the numerical results of hybrid PFFEM and classical PFFEM, respectively, when $f = 500$ Hz and $\eta = 0.01$. Since the reverberance factors of subsystems in Figs. 14 and 15 are much smaller than those in Figs. 16 and 17, the difference between the numerical results of Figs. 14 and 15 is much smaller than that between the numerical results of Figs. 16 and 17. In Figs. 14 and 15, the numerical results of hybrid PFFEM and classical PFFEM show a good agreement and their difference is not more than 1 dB. To definitely confirm the effect of reverberance factor in hybrid PFFEM for built-up structure, Fig. 18 shows the relative difference between hybrid PFFEM and classical PFFEM in the center of the roof subsystem as various reverberance factors of

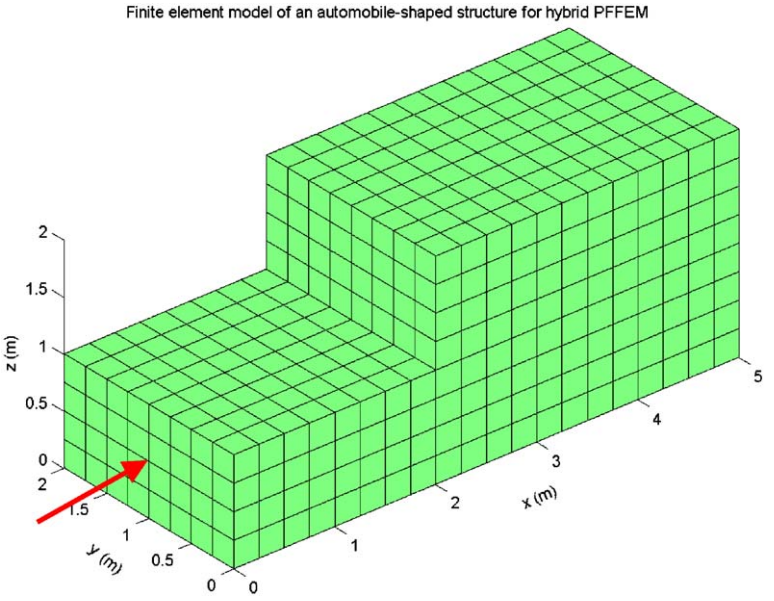

Fig. 13. Finite element model of an automobile-shaped structure for hybrid PFFEM.

the roof subsystem. Like the previous cases, as the reverberance factor of the structure decreases, the numerical results of two methods become equal. Finally, Fig. 19 shows the spatial intensity distribution that cannot be represented in classical SEA.

4. Conclusions

For the effective prediction of vibrational and acoustic responses of low-damping structures and acoustic cavities in the medium-to-high frequency ranges, the general hybrid method using the coupling relationship of SEA in PFA was derived on 3-D case besides the 1- and 2-D cases which are described in the other companion paper. Additionally, the hybrid PFFEM using the new joint element matrix including CLF of SEA was formulated to extend the region of application of hybrid PFA to built-up structures. To verify the developed methods, numerical analyses of each case were successfully performed. As a result, the hybrid power flow solutions become equivalent to the classical ones in case of not only 3-D cases but also built-up structures as the reverberance factors of the system become small.

Therefore, the developed hybrid power flow method can be a useful tool for the prediction of vibrational and acoustic responses, especially when it uses experimental coupling data for a low-damping system.

Acknowledgements

This work was partially supported by Advanced Ship Engineering Research Center of the Korea Science & Engineering Foundation.

Appendix A

The energy governing equations for 3-D acoustic cavities given in Eq. (2.1) can be expressed as,

$$-\frac{c_{g,j}^2}{\eta\omega}\left(\frac{\partial^2}{\partial x^2}+\frac{\partial^2}{\partial y^2}+\frac{\partial^2}{\partial z^2}\right)\langle e\rangle_{a,j}+\eta\omega\langle e\rangle_{a,j}=\Pi_{\mathrm{in},j}(x,y,z)\quad(j=1,2,3), \tag{A.1}$$

where $c_{g,j}$ is the group velocity of an acoustic wave, $\langle e\rangle_{a,j}$ is the acoustic energy density and $\Pi_{\mathrm{in},j}$ is the acoustic input power in cavity j. If powers transferred in all the y- and z-directional area boundaries of the cavities in

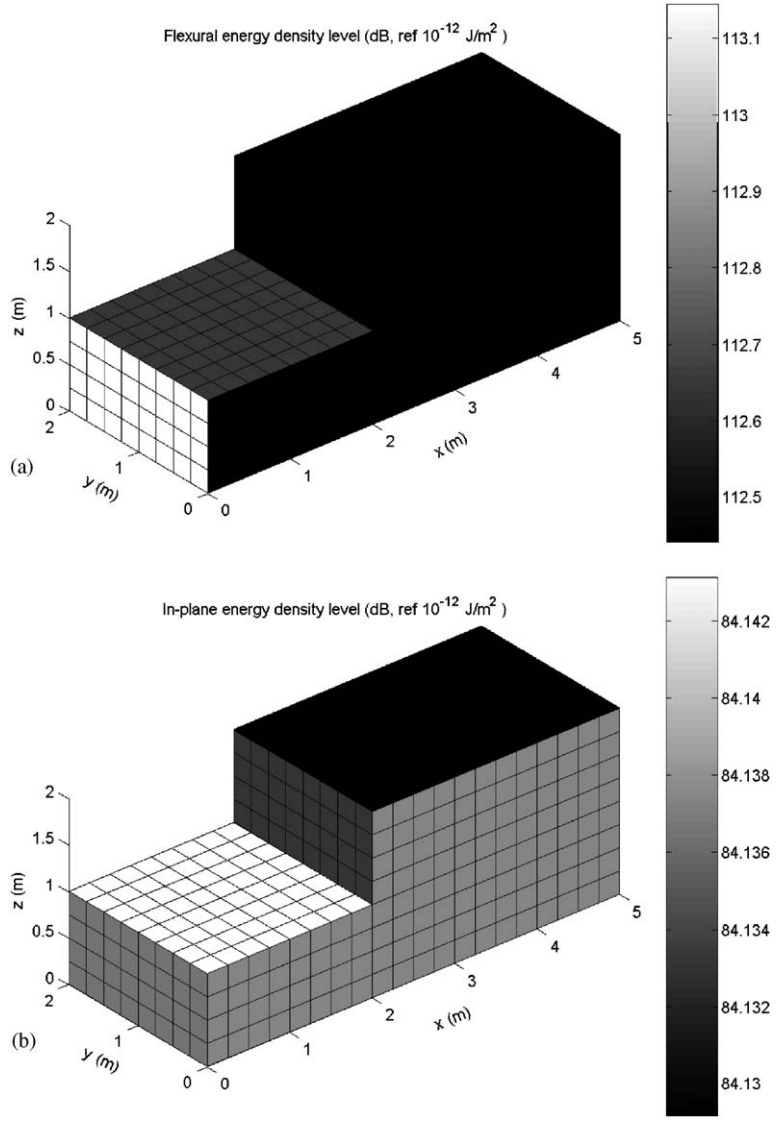

Fig. 14. Energy density levels (dB) of an automobile-shaped structure by hybrid PFFEM when $f = 200$ Hz and $\eta = 0.0001$: (a) flexural energy; and (b) in-plane energy.

the model shown in Fig. 2 are zero, the power flow solution of Eq. (A.1) can be obtained as, double series solution,

$$\langle e\rangle_{a,j}(x_j,y,z) = \sum_{m=0}^{\infty}\sum_{n=0}^{\infty}\left\{E_{j,mn}(x_j)\cos(k_m y)\cos(k_n z)\right\}$$
$$= \sum_{m=0}^{\infty}\sum_{n=0}^{\infty}\left\{(A^{+}_{j,mn}\mathrm{e}^{-\lambda_{j,mn}x_j} + A^{-}_{j,mn}\mathrm{e}^{\lambda_{j,mn}x_j})\cos(k_m y)\cos(k_n z)\right\}, \quad (A.2)$$

where $k_m = m\pi/L_y$, $k_n = n\pi/L_z$ and $\lambda^2_{j,mn} = k_n^2 + k_n^2 + (\eta_j\omega/c_{g,j})^2$.

The intensity in the jth acoustic cavity can be obtained by, using the energy transfer relation, Eq. (2.3),

$$\langle q_x\rangle_j(x_j,y,z) = \sum_{m=0}^{\infty}\sum_{n=0}^{\infty}\left\{\left(\frac{c^2_{g,j}}{\eta_j\omega}\lambda_{j,mn}\right)(A^{+}_{j,mn}\mathrm{e}^{-\lambda_{j,mn}x_j} - A^{-}_{j,mn}\mathrm{e}^{\lambda_{j,mn}x_j})\cos\, k_m y\, \cos\, k_n z\right\}, \quad (A.3)$$

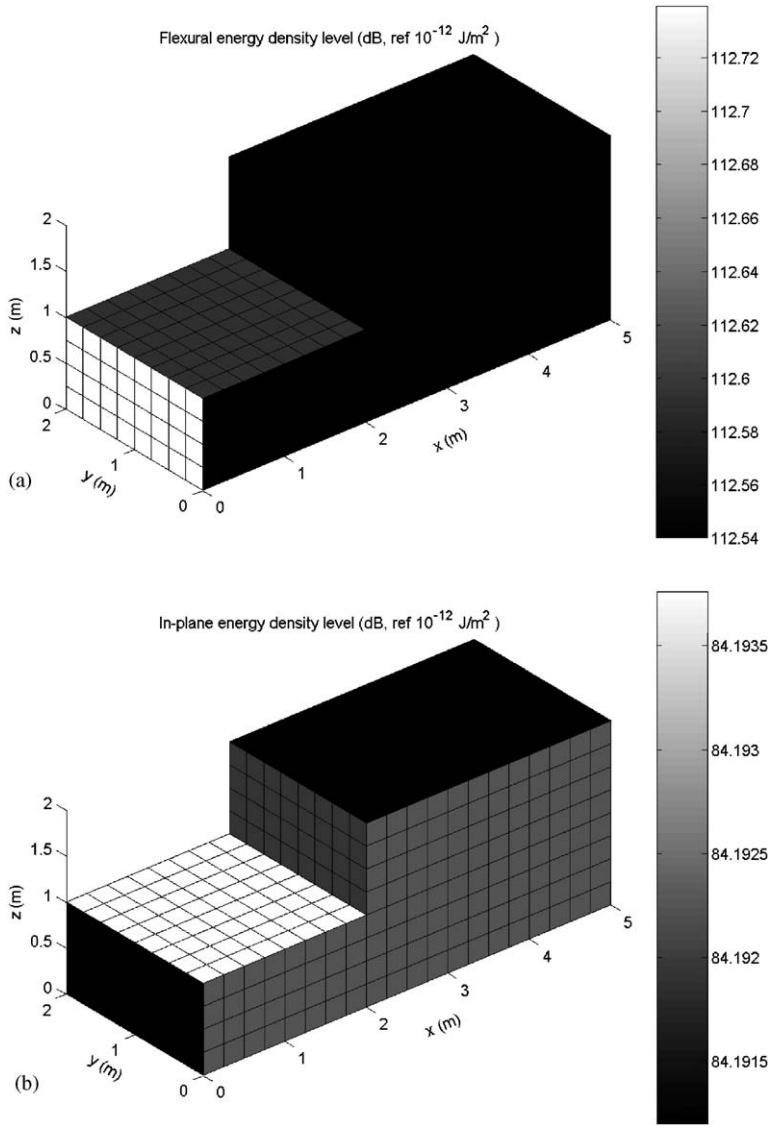

Fig. 15. Energy density levels (dB) of an automobile-shaped structure by classical PFFEM when $f = 200$ Hz and $\eta = 0.0001$: (a) flexural energy; and (b) in-plane energy.

$$\langle q_y\rangle_j(x_j,y,z)=\sum_{m=0}^{\infty}\sum_{n=0}^{\infty}\left\{\left(\frac{c_{g,j}^2}{\eta_j\omega}k_m\right)(A_{j,mn}^{+}\mathrm{e}^{-\lambda_{j,mn}x_j}+A_{j,mn}^{-}\mathrm{e}^{\lambda_{j,mn}x_j})\sin k_m y\cos k_n z\right\} \tag{A.4}$$

and

$$\langle q_z\rangle_j(x_j,y,z)=\sum_{m=0}^{\infty}\sum_{n=0}^{\infty}\left\{\left(\frac{c_{g,j}^2}{\eta_j\omega}k_n\right)(A_{j,mn}^{+}\mathrm{e}^{-\lambda_{j,mn}x_j}+A_{j,mn}^{-}\mathrm{e}^{\lambda_{j,mn}x_j})\cos k_m y\sin k_n z\right\}, \tag{A.5}$$

where $\langle q_x\rangle_j$, $\langle q_y\rangle_j$ and $\langle q_z\rangle_j$ are the x-, y- and z-components of intensity $\langle q\rangle_j$, respectively.

The input acoustic point power can be approximated as,

$$\Pi\delta(x-x_0)\delta(y-y_0)\delta(z-z_0)=\sum_{m=0}^{\infty}\sum_{n=0}^{\infty}\Pi_{mn}(x)\cos k_m y\cos k_n z, \tag{A.6}$$

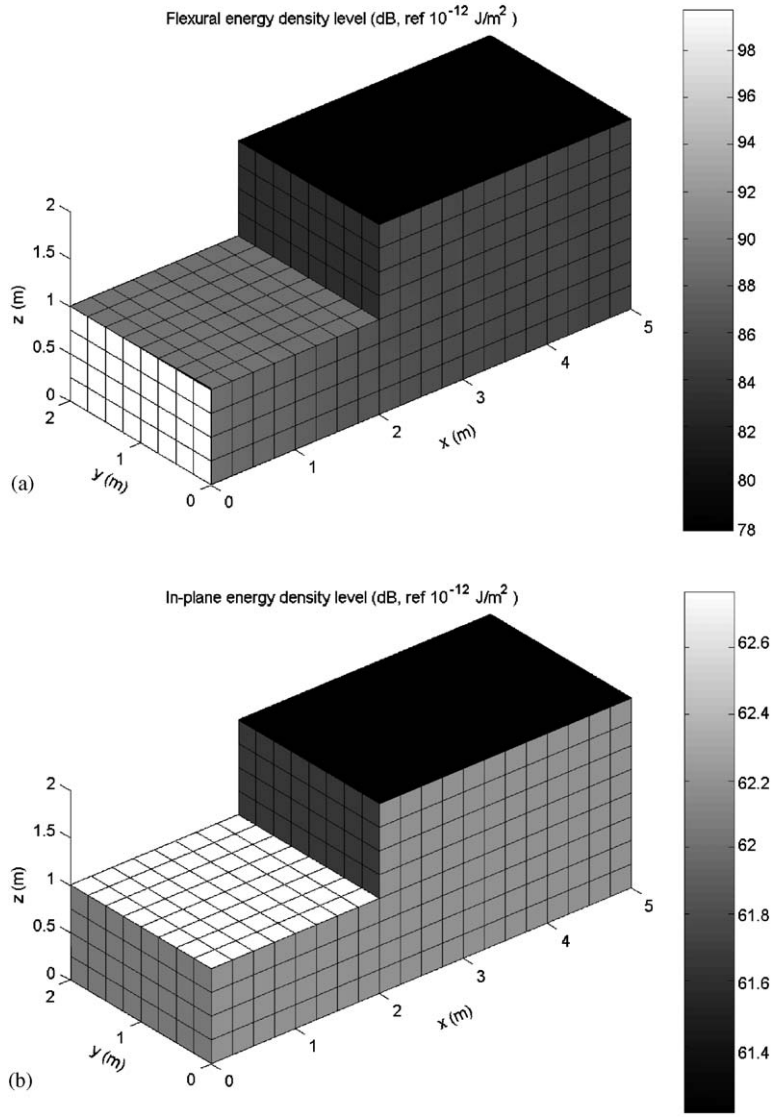

Fig. 16. Energy density levels (dB) of an automobile-shaped structure by hybrid PFFEM when $f = 500\,\text{Hz}$ and $\eta = 0.01$: (a) flexural energy; and (b) in-plane energy.

where Π is the acoustic input power. Π_{mn}, the m- and nth components of Π can be expressed as

$$\Pi_{m,n} = \begin{cases} \dfrac{\Pi}{L_y L_z}\delta(y - y_0)\delta(z - z_0) & (m = 0,\ n = 0), \\ \dfrac{2\Pi}{L_y L_z}\cos\ k_n z_0 \delta(y - y_0) & (m = 0,\ n \neq 0), \\ \dfrac{2\Pi}{L_y L_z}\cos\ k_m y_0 \delta(z - z_0) & (m \neq 0,\ n = 0), \\ \dfrac{4\Pi}{L_y L_z}\cos\ k_m y_0\ \cos\ k_n z_0 & (m \neq 0,\ n \neq 0). \end{cases} \tag{A.7}$$

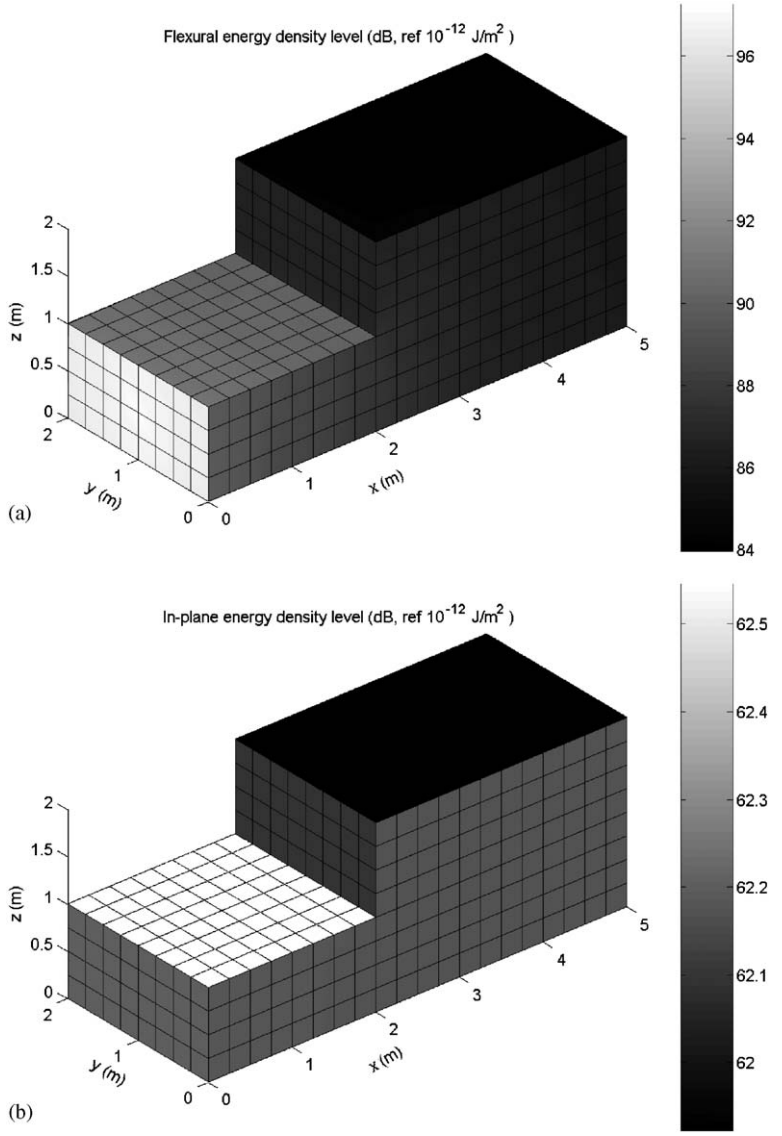

Fig. 17. Energy density levels (dB) of an automobile-shaped structure by classical PFFEM when $f = 500\,\text{Hz}$ and $\eta = 0.01$: (a) flexural energy; and (b) in-plane energy.

Two unknowns in each homogeneous acoustic cavity's domain exist and a total of eight boundary conditions must be enforced to solve the problem. The intensity of acoustic wave component is zero in the zero-power boundary, and the continuities of the energy density and intensity of each wave component in the source point must be enforced. In the area junction of coupled acoustic cavities, Eqs. (2.8) and (2.9) are applied to the classical power flow solutions and Eq. (2.7) is applied to the hybrid power flow solutions.

Appendix B. Wave transmission analysis of coupled acoustic medium

Fig. A1 shows two separated semi-infinite acoustic spaces with different characteristic specific acoustic impedances, $\rho_1 c_1$ and $\rho_2 c_2$, in the plane where x and y are zero. The incident pressure field in the semi-infinite acoustic space 1 can be represented as

$$p_{1,\text{in}}(x,z,t) = \widetilde{A}_1 \exp\left[\text{j}(\omega t - k_1 \sin\phi_1 z - k_1 \cos\phi_1 x)\right], \tag{B.1}$$

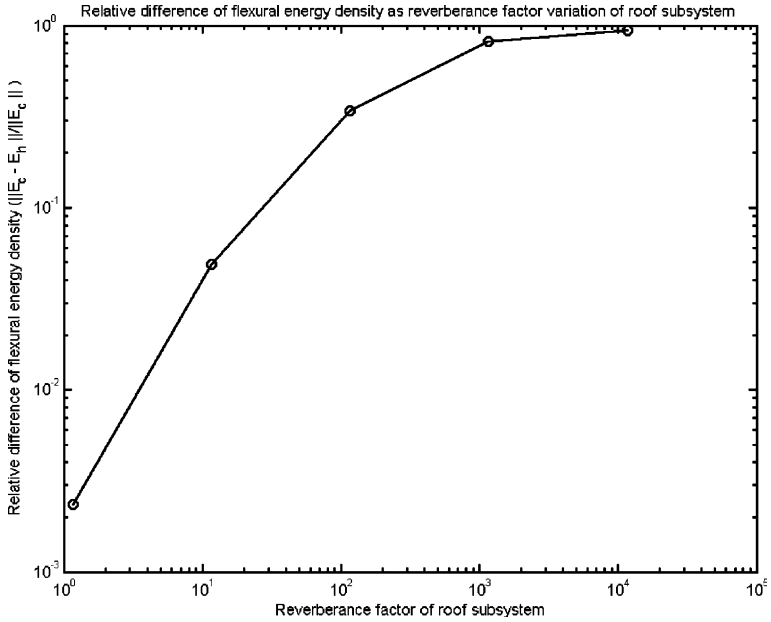

Fig. 18. Relative difference $\left(\|\overline{E_c}-\overline{E_h}\|/\|\overline{E_c}\|\right)$ between space-averaged flexural energy densities of the roof subsystem, by classical and hybrid PFFEM as the reverberance factor variation of the roof subsystem.

where $\widetilde{A}_1$ is the amplitude of the incident pressure in acoustic space 1, ϕ_1 are the incident angle and $k_1=\omega/c_1$. The pressure field of the reflected wave from the boundary is written by

$$p_{1,\,\mathrm{ref}}(x,z,t)=\widetilde{B}_1\,\exp\left[\mathrm{j}(\omega t-k_1\,\sin\,\phi_1 z+k_1\,\cos\,\phi_1 x)\right]. \tag{B.2}$$

The acoustic pressure field transmitted in the $+x$-direction can be represented as

$$p_{2,\,\mathrm{tran}}(x,z,t)=\widetilde{A}_2\,\exp\left[\mathrm{j}(\omega t-k_2\,\sin\,\phi_2 z-k_2\,\cos\,\phi_2 x)\right]. \tag{B.3}$$

Since the acoustic waves on both sides of the boundary share the same wave motion along the boundary, the following equation is confirmed:

$$k_1\,\sin\,\phi_1=k_2\,\sin\,\phi_2 \tag{B.4}$$

which is the Snell's Law. Therefore, when Eq. (B.4) is substituted into Eq. (B.3), the acoustic pressure field in space 1 can be represented as

$$p_{2,\,\mathrm{tran}}(x,z,t)=\widetilde{A}_2\,\exp\left[\mathrm{j}\left(\omega t-k_1\,\sin\,\phi_1 z-k_1\sqrt{(k_2/k_2)^2-\sin^2\phi_1}\,x\right)\right], \tag{B.5}$$

where the incident angle is smaller than critical angle, $\phi_c=\sin^{-1}(k_2/k_1)$. When $\phi_1>\phi_c$, the incident wave is totally reflected, this results in a transmitted, exponentially decaying wave. Hence, the resulting acoustic pressure field can be represented as

$$p_{2,\,\mathrm{tran}}(x,z,t)=\widetilde{A}_2\,\exp\left[\mathrm{j}\left(\omega t-k_1\,\sin\,\phi_1 z-\mathrm{j}k_1\sqrt{\sin^2\phi_1-(k_2/k_1)^2}\,x\right)\right]. \tag{B.6}$$

Because the velocity and pressure matching boundary conditions are enforced, the following relations can be obtained as, by Euler's equation, respectively,

$$p_{1,\,\mathrm{in}})_{x=-0}+p_{1,\,\mathrm{ref}})_{x=-0}=p_{2,\,\mathrm{tran}})_{x=+0} \tag{B.7}$$

and

$$\frac{-1}{\mathrm{j}\omega\rho_1}\left\{\left(\frac{\partial p_{1,\,\mathrm{in}}}{\partial x}\right)_{x=-0}+\left(\frac{\partial p_{1,\,\mathrm{ref}}}{\partial x}\right)_{x=-0}\right\}=\frac{-1}{\mathrm{j}\omega\rho_2}\left(\frac{\partial p_{2,\,\mathrm{tran}}}{\partial x}\right)_{x=+0}. \tag{B.8}$$

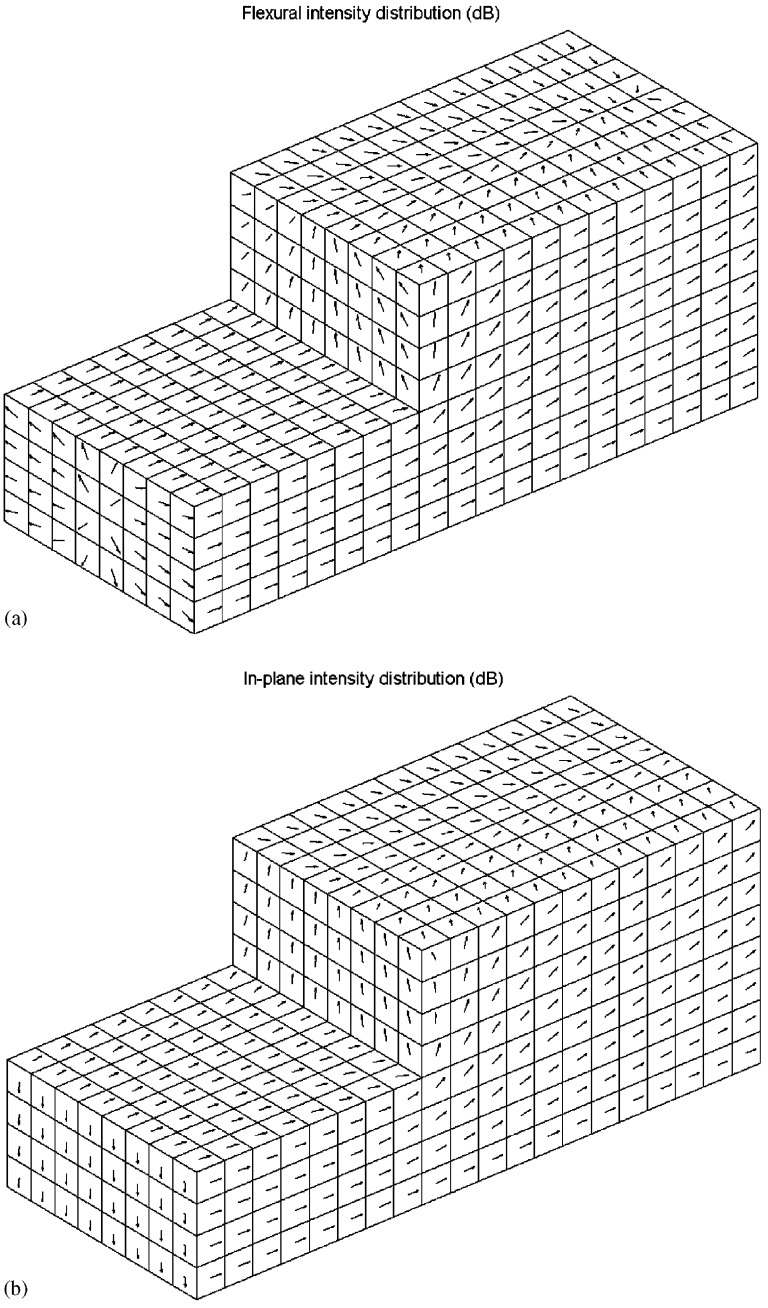

Fig. 19. Intensity level distribution (dB) of an automobile-shaped structure by classical PFFEM when $f = 500\,\text{Hz}$ and $\eta = 0.01$: (a) flexural energy; and (b) in-plane energy.

By the upper boundary conditions, the amplitudes of the transmitted and reflected pressure fields can be expressed in terms of those of the incident pressure field, when $\phi_1 < \phi_c$:

$$\widetilde{A}_2 = \frac{\left(2\cos\phi_1/(\rho_1 c_1)\right)}{\left(\cos\phi_1/(\rho_1 c_1) + \sqrt{1-(c_2\sin\phi_1/c_1)^2}/(\rho_2 c_2)\right)}\widetilde{A}_1 \tag{B.9}$$

and

$$\widetilde{B}_1 = \frac{\left(\cos\,\phi_1/(\rho_1 c_1) - \sqrt{1-(c_2\sin\,\phi_1/c_1)^2}/(\rho_2 c_2)\right)}{\left(\cos\,\phi_1/(\rho_1 c_1) + \sqrt{1-(c_2\sin\,\phi_1/c_1)^2}/(\rho_2 c_2)\right)}\widetilde{A}_1. \tag{B.10}$$

The time-averaged acoustic energy density can be represented as the sum of the kinetic and potential energy densities:

$$\langle e\rangle_a = \frac{1}{4}\rho_0\left[\vec{u}\cdot\vec{u}^* + \frac{pp^*}{(\rho_0 c_0)^2}\right]. \tag{B.11}$$

The acoustic intensity can be represented as

$$\langle\vec{I}\rangle_a = \frac{1}{2}\,\mathrm{Re}\{p^*\vec{u}\}. \tag{B.12}$$

The sound power transmission and reflection coefficients can be expressed as, by considering the refraction of waves, respectively,

$$\tau(\phi_1) = \frac{\left|\widetilde{A}_2\right|^2\Big/2\rho_2 c_2}{\left|\widetilde{A}_1\right|^2\Big/2\rho_1 c_1}\frac{\cos\,\phi_2}{\cos\,\phi_1} = \frac{4\rho_1 c_1\rho_2 c_2\sqrt{1-\sin^2\phi_1}\sqrt{1-(c_2\,\sin\,\phi_1/c_1)^2}}{\left|\rho_2 c_2\sqrt{1-\sin^2\phi_1}+\rho_1 c_1\sqrt{1-(c_2\,\sin\,\phi_1/c_1)^2}\right|^2} \tag{B.13}$$

and

$$\gamma(\phi_1) = \frac{\left|\widetilde{B}_1\right|^2\Big/2\rho_1 c_1}{\left|\widetilde{A}_1\right|^2\Big/2\rho_1 c_1}\frac{\cos\,\phi_1}{\cos\,\phi_1} = \frac{\left|\rho_2 c_2\sqrt{1-\sin^2\phi_1}-\rho_1 c_1\sqrt{1-(c_2\,\sin\,\phi_1/c_1)^2}\right|^2}{\left|\rho_2 c_2\sqrt{1-\sin^2\phi_1}+\rho_1 c_1\sqrt{1-(c_2\,\sin\,\phi_1/c_1)^2}\right|^2}. \tag{B.14}$$

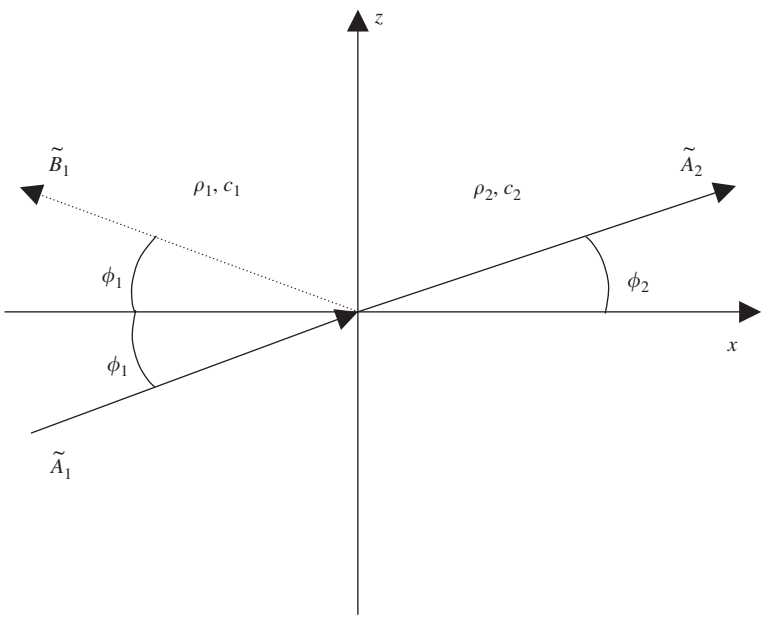

Fig. A1. Transmission of obliquely incident sound from medium 1 to medium 2.

The diffuse sound transmission and reflection coefficients can be expressed as, by considering 3-D space, respectively [10],

$$\langle\tau\rangle = \frac{\int_0^{\pi/2} \tau(\phi) \sin\,\phi\,\cos\,\phi\,\mathrm{d}\phi}{\int_0^{\pi/2} \sin\,\phi\,\cos\,\phi\,\mathrm{d}\phi} = \int_0^{\pi/2} \tau(\phi) \sin\,2\phi\,\mathrm{d}\phi \tag{B.15}$$

and

$$\langle\gamma\rangle = \frac{\int_0^{\pi/2} \gamma(\phi) \sin\,\phi\,\cos\,\phi\,\mathrm{d}\phi}{\int_0^{\pi/2} \sin\,\phi\,\cos\,\phi\,\mathrm{d}\phi} = \int_0^{\pi/2} \gamma(\phi) \sin\,2\phi\,\mathrm{d}\phi, \tag{B.16}$$

where the sum of the diffuse transmission and reflection coefficients is 1. To evaluate the diffuse power transmission and reflection coefficients of Eqs. (B.15) and (B.16), the numerical methods are needed.

References

[1] Y.-H. Park, S.-Y. Hong, Hybrid power flow analysis using coupling loss factor of SEA for low-damping system—Part I: formulation of 1-D and 2-D cases, *Journal of Sound and Vibration*, this issue.

[2] R.H. Lyon, R.G. DeJong, *Theory and Application of Statistical Energy Analysis*, second ed., Butterworth-Heinemann, Stoneham, MA, 1995.

[3] O.H. Bouthier, R.J. Bernhard, Models of spaced-averaged energetics of plates, *AIAA Journal* 30 (3) (1992) 616–623.

[4] O.H. Bouthier, The Energetics of Plates, PhD Dissertation, Purdue University, 1992.

[5] D.J. Nefske, S.H. Sung, Power flow finite element analysis of dynamic systems: basic theory and application to beams, *Journal of Vibration, Acoustics, Stress, and Reliability in Design* 111 (1989) 94–100.

[6] P.E. Cho, Energy Flow Analysis of Coupled Structures, PhD Thesis, Purdue University, 1993.

[7] S.-H. Seo, Power Flow Finite Element Method for the Various Plate Structures in Shape, Master Thesis, Seoul National University, 2000.

[8] S.-H. Seo, S.-Y. Hong, Y.-H. Park, Development of PFFEM software—"PFADS R3": (I) program structures and functions, *Proceedings of Internoise2003*, Jeju, August 2003.

[9] Y.-H. Park, S.-Y. Hong, S.-H. Seo, Development of PFFEM software—"PFADS R3": (II) applications to vehicle vibration analysis, *Proceedings of the Internoise2003*, Jeju, August 2003.

[10] F.J. Fahy, *Sound and Structural Vibration: Radiation, Transmission and Response*, Academic Press, New York, 1985.